

## Multicolor photometry of 145 of the HII regions in M33

Linhua Jiang<sup>1,2</sup>, Jun Ma<sup>1</sup>, Xu Zhou<sup>1</sup>, Jiansheng Chen<sup>1</sup>, Hong Wu<sup>1</sup>, Zhaoji Jiang<sup>1</sup>, Suijian Xue<sup>1</sup>, and Jin Zhu<sup>1</sup>

Received \_\_\_\_\_; accepted \_\_\_\_\_

---

<sup>1</sup>National Astronomical Observatories of CAS and CAS-Peking University joint Beijing Astronomical Center, Beijing, 100012, P. R. China

<sup>2</sup>Department of Astronomy, Peking University, Beijing, 100871, P. R. China

## ABSTRACT

This paper is the first in a series presenting CCD multicolor photometry for 145 HII regions, selected from 369 candidate regions from Boulesteix et al. (1974), in the nearby spiral galaxy M33. The observations, which covered the whole area of M33, were carried out by the Beijing Astronomical Observatory 60/90 cm Schmidt Telescope, in 13 intermediate-band filters, covering a range of wavelength from 3800 to 10000Å. This provides a series of maps which can be converted to a multicolor map of M33, in pixels of  $1''.7 \times 1''.7$ . Using aperture photometry we obtain the spectral energy distributions (SEDs) for these HII regions. We also give their identification charts. Using the relationship between the BATC intermediate-band system used for the observations and the *UBVRI* broad-band system, the magnitudes in the *B* and *V* bands are then derived. Histograms of the magnitudes in *V* and in *B*–*V* are plotted, and the color-magnitude diagram is also given. The distribution of magnitudes in the *V* band shows that the apparent magnitude of almost all the regions is brighter than 18, corresponding to an absolute magnitude of  $-6.62$  for an assumed distance modulus of 24.62, which corresponds to a single main sequence O5 star, while the distribution of color shows that the sample is blue, with a mode close to  $-0.05$  as would be expected from a range of typical young clusters.

*Subject headings:* galaxies: individual (M33) – galaxies: evolution – galaxies: HII regions

## 1. INTRODUCTION

HII regions provide an excellent means of studying the ongoing and accumulated star formation in a late type galaxy. In a well-resolved galaxy, HII regions can offer much useful information: about the current status of star formation, and the physical conditions in the interstellar medium near the hot young stars within the galaxy (see e.g., Wyder, Hodge, & Skelton 1997), and it is well established that observations of extragalactic HII regions are important for the understanding of the chemical evolution and star formation history of the parent galaxy. For these purposes HII regions in many nearby galaxies have been explored in considerable detail (Garnett & Shields 1987), which include M31 (Baade & Arp 1964; Pellet et al. 1978; Walterbos & Braun 1992; Walterbos 2000), and M81 (Garnett & Shields 1987; Petit, Sivan, & Karachentsev 1988; Hill et al. 1995; Miller & Hodge 1996).

M33, one of our two nearest spiral neighbors, is a small Scd Local Group galaxy, whose distance modulus, determined via its Cepheids by Freedman, Wilson and Madore (1991), was more recently revised to 24.62 by Freedman et al. (2001). Because it is so near, and has quite a low inclination ( $\sim 33^\circ$ ), M33 is an excellent candidate for HII region studies. A good database for its star clusters has been built up from the ground-based work (Hiltner 1960; Kron & Mayall 1960; Melnick & D'Odorico 1978; Christian & Schommer 1982, 1988), and from the *Hubble Space Telescope (HST)* images (Chandar, Bianchi, & Ford 1999a, 1999b; Chandar, Bianchi, & Ford 2001). Ma et al. (2001, 2002a, 2002b) obtained the spectral energy distributions (SEDs) of 144 star clusters, and estimated their ages by comparing the photometry of each object with theoretical stellar population synthesis models for different values of metallicity.

The HII regions in M33 have proved of interest to astronomers for well over half a century (see e.g., Aller 1942, Haro 1950, Courtès & Cruvellier 1965). Aller (1942) used the ratio of  $[\text{OIII}] \lambda 5007 / [\text{OII}] \lambda 3727$  to be the criterion for identifying HII regions. However, most studies searched HII regions by photographic  $H\alpha$  survey. In 1974, Boulesteix et al. (1974) compiled a major catalogue of 369 distinct HII regions by a complete photographic  $H\alpha$  survey of M33. In this study, Boulesteix et al. (1974) defined an HII region within the  $H\alpha$  image of M33 to correspond to an emission measure of  $150 \text{ cm}^{-6}\text{pc}$ , i.e. three times above the rms noise level. Later Courtès et al. (1987) added an additional 410 objects to that catalogue, also using a photographic  $H\alpha$  survey, and defined an HII region within the  $H\alpha$  image of M33 to correspond to an emission measure of  $40 \text{ cm}^{-6}\text{pc}$ . In a paper in which they selected isolated candidates for SS433-like stellar systems, Calzetti et al. (1995) reported 432 compact regions emitting  $H\alpha$ . Recently a more extensive catalogue with 2338  $H\alpha$  emission regions of M33 was published by Hodge et al. (1999). While these authors made an explicit position and luminosity catalogue, others paid more attention to the luminosity function and size distribution of the HII regions on the basis of  $H\alpha$  surveys (e.g., Wyder et al. 1997, Cardwell et al. 2000). The latter authors claim to have identified over 10000 separate HII regions in  $H\alpha$ , but so far have not published a catalogue.

Although there is already much observational information in the literature, for full physical information about the HII regions it is of great value to obtain multiband photometry, which can provide accurate SEDs. In the present study we present CCD spectrophotometry of a set of HII regions in M33 using images obtained with the Beijing-Arizona-Taiwan-Connecticut (BATC) Multicolor Sky Survey Telescope, designed to obtain SED information for galaxies (Fan et al. 1996). The BATC system uses the 60/90 cm Schmidt telescope with 15 intermediate bandwidth filters. Here we use 13 of these filters, from 3800 to 10000Å, with images covering the whole visible extent of M33. In this paper we present the SEDs of 145 HII regions selected from the sample of Boulesteix et al. (1974), and also supply identification charts for these regions. We go on to compute the  $B$  and  $V$  magnitudes for these regions, using previously derived relationships between the BATC intermediate band system and the  $UBVRI$  broad-band system. Finally we plot histograms of the  $V$  band magnitudes and also of  $B-V$ , as well as plotting the corresponding color-magnitude diagram for our sample regions.

We note that the extinction for almost all of the HII regions remains undetermined. Although it has been derived for a few of the large regions (Viallefond, Donas, & Goss 1983; Viallefond & Goss 1986; Churchwell & Goss 1999), the extinction for the regions sampled here has not been previously presented. In M81 the extinction varies relatively little from HII region to HII region (Hill et al. 1995), but in M33 there is considerable variation (Viallefond, Donas & Goss 1983). We cannot use the assumption of uniform extinction to correct for reddening in the present paper, so we have not been able to infer the intrinsic fluxes of the regions. In a forthcoming article (Jiang et al. 2002) we will use the flux ratio of  $H_\alpha/H_\beta$  to study the extinction region by region.

The outline of this paper is as follows: details of the observations and data reduction are given in section 2. In section 3 we give the SEDs and the identification charts for the 145 regions studied. In this section also we produce the histograms of the  $V$  magnitude, and of  $B-V$ , as well as the color-magnitude diagram. Finally in section 4 we give a summary.

## 2. SAMPLE OF HII REGIONS, OBSERVATIONS AND DATA REDUCTION

### 2.1. Selection of the Sample

The sample of HII regions chosen for this paper comes from the catalogue of 369 HII regions by Boulesteix et al. (1974). Courtès et al. (1987) added an additional 410 objects to this catalogue. We take regions from Boulesteix's catalogue as our sample, while we use positions and sizes available from Courtès et al. (1987), because positions presented by Courtès et al. (1987) are more accurate than those given by Boulesteix et al. (1974) (spatial resolutions are about 1'' and 4'' respectively). We set out to observe all the Boulesteix regions, but found that for 224 of these the signal-to-noise ratio achieved was not sufficient in at least some of the filters, so we have eliminated these from the final sample presented. For this purpose we used the criterion that a region with a photometric uncertainty in any filter of more than 1 magnitude was not suitable for analysis. This criterion rejects the least luminous regions, which makes our sample regions somewhat bright (see section 3 and Fig. 1). At last the 145 HII regions which passed this limit test are included here.

### 2.2. BATC Observations

As M33 is so near, it subtends a large angle on the sky, which makes it non-trivial to obtain CCD images over the whole disk (Walterbos 2000). This difficulty can be resolved with an instrument with a large field format. The BATC telescope and filter system is well suited to this type of observations. The telescope is a 60/90 cm f/3 Schmidt, belonging to the Beijing Astronomical Observatory (BAO) at the Xinglong station. A Ford Aerospace 2048×2048 CCD camera, with 15  $\mu\text{m}$  pixel size is mounted at the Schmidt focus, giving a field of view of 58' × 58' with a pixel size of 1.7''.

The multiband BATC filter system comprises 15 intermediate-band filters, covering the full optical wavelength range from 3000 to 10000Å. The filters were designed specifically to avoid contamination from the brightest and most variable night sky emission lines. Details of the BAO Schmidt Telescope, the CCD camera, the data acquisition system, and the definition of the BATC filter passbands can be found in previous publications (Fan et al. 1996; Zheng et al. 1999). The observations of M33 were carried out from September 23, 1995, through August 28, 2000, with a total exposure time of about 38 hr 15 min. The CCD images, which were centered at RA = 01<sup>h</sup>33<sup>m</sup>50.58 and DEC=30°39'08.4" (J2000) covered the full optical extent of M33, imaging this in 13 of the BATC filters. The dome flats were obtained using a diffusor plate in front of the Schmidt corrector plate. For flux calibration the Oke-Gunn primary standard stars HD 19445, HD 84937, BD +26°2606, and BD +17°4708 were observed under photometric conditions (see Yan et al. 2000, Zhou et al. 2001 for details). The parameters of the filters, and the basic statistics of the observations are given in Table 1.

Table 1: Parameters of the BATC filters and statistics of observations

No.	Name	cw <sup>a</sup> (Å)	Exp. (hr)	N.img <sup>b</sup>	rms <sup>c</sup>
1	BATC03	4210	00:55	04	0.024
2	BATC04	4546	01:05	04	0.023
3	BATC05	4872	03:55	19	0.017
4	BATC06	5250	03:19	15	0.006
5	BATC07	5785	04:38	17	0.011
6	BATC08	6075	01:26	08	0.016
7	BATC09	6710	01:09	08	0.006
8	BATC10	7010	01:41	08	0.005
9	BATC11	7530	02:07	10	0.017
10	BATC12	8000	03:00	11	0.003
11	BATC13	8510	03:15	11	0.005
12	BATC14	9170	05:45	25	0.011
13	BATC15	9720	06:00	26	0.009

<sup>a</sup>Central wavelength for each BATC filter<sup>b</sup>Image numbers for each BATC filter<sup>c</sup>Zero point error, in magnitude, for each filter as obtained from the standard stars

### 2.3. Data Reduction

Using standard procedures, which include bias subtraction and flat-fielding of the CCD images, the data were reduced by automatic reduction software: PIPELINE I, developed for the BATC multicolor sky survey (Fan et al. 1996; Zheng et al. 1999). Flat-fielded images for a given band were combined by integer pixel shifting. The images were re-centered and position calibrated, basing the astrometry on stars from the *HST* Guide Star Catalogue. The technique of integer pixel shifting is somewhat rather crude for registering images, since a pixel corresponds to 1''.7. However, as M33 is quite close, 1''.7 does not amount to a major fraction of the radius of a large HII region. Cosmic rays and bad pixels were corrected by comparison between images during combination. The images were calibrated using observations of standard stars, having convolved the SEDs of these stars with the measured BATC filter transmission functions (Fan et al. 1996), to derive the fluxes of these Oke-Gunn standards as observed through the BATC filters. In Table 1, *Column 6* gives the zero point errors in magnitude for the standard stars through each filter. The formal errors obtained for these stars in the 13 BATC filters used are  $\lesssim 0.02$  mag, which implies that we can define photometrically the BATC system to an accuracy of better than 0.02 mag.

### 3. RESULTS

#### 3.1. Integrated Photometry

To obtain the magnitude of a given HII region, we used aperture photometry. The HII regions have a variety of shapes: disks, loops, arcs, and filaments, and a considerable range of sizes (see Courtès et al. 1987). We followed the specifications of Courtès et al. who presented measured sizes in two orthogonal coordinates: the E-W extent, and the N-S extent, for all regions; we used the larger of these as the aperture for our photometric measurements. As the HII regions are found in a variety of local environments, background subtraction is not straightforward. We determined the background within an annular aperture for each region. Within the chosen annulus we fitted each pixel row of the image by a linear median, obtaining a surface, and repeated this process in the column direction with this surface. After this, we rejected points which differed from the mean background by over 30%, and derived a smoothed background fit as the final step. Using this background surface, we made the background subtraction for each HII region. We used a standard set of ratios between the aperture radius for a given region, and the inner and outer radii of its background annuli; these ratios are specified in Table 2, where *Column 1* lists a set of aperture ranges in pixels, while *Column 2* and *3* give the corresponding inner and outer radii for the background apertures. For example, if an HII region is 30 pixels in size (diameter), i.e. photometric aperture radius is 15, which is more than 10 and less than 20, then the inner radius of its background annulus is  $15 + 15 = 30$ , and the outer radius,  $15 + 25 = 40$ . Using these parameters and the method outlined, the backgrounds were obtained and subtracted for the complete set of HII regions in each filter.

Table 2: The relationships between the range of the photometric aperture size and the inner and outer sizes of its background annulus

Radius of photometric aperture (r)	Inner radius of annulus	Outer radius of annulus
$\leq 5$	r+5	r+15
$5 \sim 10$	r+10	r+20
$10 \sim 20$	r+15	r+25
$20 \sim 30$	r+20	r+30
$30 \sim 40$	r+25	r+35
$40 \sim 50$	r+30	r+40
$\geq 50$	r+40	r+50

Finally we used the fluxes in the filters to derive the SEDs for the 145 HII regions, which are listed in Table 3. This contains the following information: *Column 1* is a check number for each HII region, taken from Boulesteix et al. (1974), *Column 2* through *14* show the magnitudes in the selected BATC bands, and

on a second row for each HII region in these columns we give the magnitude uncertainty for each band. These uncertainties include the errors from the object count rate, the sky variance, and the instrument gain.

### 3.2. Magnitudes in the B and V Bands, and (B–V) Colors

Using Landolt standards, Zhou et al. (2002) derived the relationships between the BATC intermediate band system and the *UBVRI* broad-band system, making use of the catalogues of Laondolt (1983, 1992), and of Galadí-Enríquez et al. (2000). The relationships are given in equations (1) and (2) as :

$$m_B = m_{04} + (0.2218 \pm 0.033)(m_{03} - m_{05}) + 0.0741 \pm 0.033, \quad (1)$$

$$m_V = m_{07} + (0.3233 \pm 0.019)(m_{06} - m_{08}) + 0.0590 \pm 0.010. \quad (2)$$

Using equations (1) and (2) we transformed the magnitudes of the 145 HII regions in the BATC03, BATC04 and BATC05 bands into *B* band magnitudes, and also derived *V* band magnitudes from those in BATC06, BATC07 and BATC08. HII regions in general have strong emission lines, and in the bands chosen here, the BATC05 band can be significantly affected. In those cases where there is a strong emission line in the BATC05 band, it is suited to interpolate between the BATC04 and BATC06 bands to substitute the BATC05 band. Here we take the mean value between BATC04 and BATC06 as the value of BATC05 to calculate the *B* magnitude, when there is strong emission line in the BATC05 band.

In Figure 1 we give a histogram of the distribution of magnitudes in the computed *V* band. As is mentioned previously, our criterion of choosing the sample rejects the least luminous HII regions (see section 2.1 for a detail), and it makes our sample regions somewhat bright. From this figure we can see that almost all of our sample of HII regions are brighter than 18th magnitude, and using a distance modulus for the galaxy of 24.62 (Freedman et al. 2001) this corresponds to an absolute magnitude in *V* of −6.62. This is the equivalent of a single main sequence O5 star, and although the stars within different HII regions may differ in their mass distribution, this gives us an idea of the observational limits of our data set. In fact, it is generally accepted that the bright HII regions are ionized by several to hundreds of young massive stars (see e.g., Kennicutt 1988; Kennicutt & Chu 1988; Mayya 1994; Oey & Kennicutt 1997), especially O stars, and O5 stars may be the most typical (see e.g., Kennicutt 1984; Kennicutt 1988; Kennicutt & Chu 1988; Mayya 1994), whose magnitudes are exactly the lower magnitude limit of our sample regions. For example, taking the bright HII regions in nearby galaxies as his research sample, Kennicutt (1984, 1998) gave the equivalent number of O5 *V* stars which would be required to ionize the sample regions, and found that the number ranged from a few to about a thousand. Here we take the brightest HII region in M33, NGC604 (No. 608 in this text), as a sample to compute the equivalent number of O5 stars which would ionize the region. Using equation (2) we get *V* magnitude of NGC604, 12.40, which corresponds to an absolute *V* magnitude of −12.22. By comparing this value with *V* magnitude of a single main sequence O5 star, we

get the equivalent number of O5 stars in NGC604, 174. This result is well in agreement with one given by Hunter et al. (1996), 186 O stars, and also in the range between 150 and 215 derived by González Delgado (2000).

We present the distribution of the HII regions in our computed  $B-V$  colors in Figure 2. We can see that in general the regions are quite blue, i.e. the colors of 90% sample HII regions are bluer than 0.4, with a mode close to  $-0.05$  as expected for zones whose light is dominated by stars in young clusters. In fact, Kennicutt et al. (1988) defined the blue populous clusters in M33 to be those with  $B-V \lesssim 0.5$ . If so, most of our sample regions are dominated by young blue clusters, as is already expected. By photometry in  $BVR$  continuum bands and in the emission line of  $H\alpha + [\text{NII}]$ , Mayya (1994) derived  $B-V$  colors for 186 HII regions in 9 galaxies, and found that the colors of the most sample regions are between  $-0.2$  and  $0.5$ , and the median value is  $0.21$ . It is obvious that our sample HII regions are typical as those of Mayya (1994). The color-magnitude diagram,  $V$  against  $B-V$ , is shown in Figure 3.

### 3.3. The SEDs and the HII region identification charts

The SEDs for each of the HII regions observed are plotted in Figure 4. For convenience, we calculated the ratio of the flux in each filter to the flux in filter BATC08, and these ratios are shown as values of y-axis in Figure 4. From this figure, we can see that many of the HII regions have strong emission lines, which show up in the BATC05, BATC09 and BATC14 bands. These lines clearly correspond to [OIII] at  $5007\text{\AA}$ , the combination of  $H\alpha$  at  $6563\text{\AA}$  and the [NII] doublet surrounding it, and the [SIII] line at  $9069\text{\AA}$  respectively.

In Figure 5, we give identification charts for all of the HII regions observed in the BATC07 band, using positions from Courtès et al. (1987). The diameter of the circle gives the diameter of the photometric aperture used in each case. Where a region is not included in the catalogue of Courtès et al. (1987) we used positions and effective radii from Boulesteix et al. (1974). For clarity, in Fig. 6 we have divided the image of M33 from Fig. 5 into ten subfields, and have provided an amplified version of the finding chart in the 10 separate subfields used.

## 4. SUMMARY

Using images of M33 obtained with the Beijing-Arizona-Taiwan-Connecticut (BATC) multi-band Sky Survey Telescope, we present CCD spectrophotometry of HII regions in this galaxy. The main result is the spectral energy distributions (SEDs) of 145 HII regions, catalogued by Boulesteix et al. (1974), for which we also provide identification charts. We have been able to use the information in the 13 intermediate bands observed to transform to  $V$  magnitude and  $B-V$  color, using previously derived relationships between the

BATC system and the *UBVRI* system. We have plotted histograms of the distribution of the  $V$  magnitudes and the  $B-V$  colors, as well as a  $V$  versus  $B-V$  color-magnitude diagram for the 145 regions studied. Information on the observational limitation of the present survey can be inferred from the fact that virtually all the regions studied have apparent magnitude 18 or brighter, and from the  $B-V$  histogram we can infer that the regions observed are generally quite blue, as expected for zones whose dominant light sources are young clusters.

We would like to thank the anonymous referee for his/her insightful comments and suggestions that improved this paper. We are also indebted to him for English editing. The work is supported partly by the National Sciences Foundation under the contract No. 19833020 and No. 19503003. The BATC Survey is supported by the Chinese Academy of Sciences, the Chinese National Natural Science Foundation and the Chinese State Committee of Sciences and Technology. The project is also supported in part by the National Science Foundation (grant INT 93-01805) and by Arizona State University, the University of Arizona and Western Connecticut State University.

## REFERENCES

- Aller, L. H. 1942, ApJ, 95, 52
- Baade, W., & Arp, H. 1964, ApJ, 139, 1027
- Boulesteix, J., Courtès, G., Laval, A., Monnet, G., & Petit, H. 1974, A&A, 37, 33
- Calzetti, D., Kinney, A. L., Ford, H., Doggett, J., & Long, K. S. 1995, AJ, 110, 2739
- Cardwell, A., Beckman, J. E., Magrini, L., & Zurita, A. 2000, The Interstellar Medium in M31 and M33, Proceedings 232, 115
- Chandar, R., Bianchi, L., & Ford, H. C. 1999a, ApJS, 122, 431
- Chandar, R., Bianchi, L., & Ford, H. C. 1999b, ApJ, 517, 668
- Chandar, R., Bianchi, L., & Ford, H. C. 2001, A&A, 366, 498
- Christian, C. A., & Schommer, R. A. 1982, ApJS, 49, 405
- Christian, C. A., & Schommer, R. A. 1988, AJ, 95, 704
- Churchwell, E., & Goss, W. M. 1999, ApJ, 514, 188
- Courtès, G., & Cruvelli, P. 1965, Ann. Astrophys., 28, 683
- Courtès, G., Petit, H., Sivan, J. P., Dodonov, S., & Petit, M. 1987, A&A, 174, 28
- Fan, X., et al. 1996, AJ, 112, 628
- Freedman, W. L., et al. 2001, ApJ, 553, 47
- Freedman, W. L., Wilson, C. D., & Madore, B. F. 1991, ApJ, 372, 455
- Galadí-Enríquez, D., Trullols, E., & Jordi, C. 2000, A&AS, 146, 169
- Garnett, D. R., & Shields, G. A. 1987, ApJ, 317, 82
- González Delgado, R. M., & Pérez, E. 2000, MNRAS, 317, 64
- Haro, G. 1950, AJ, 55, 66
- Hill, J. K., et al. 1995, ApJ, 438, 181
- Hiltner, W. A. 1960, ApJ, 131, 163

Hodge, P. W., Balsley, J., Wyder, T. K., & Skelton, B. P. 1999, PASP, 111, 685

Hunter, D. A., Baum, W. A., O’Neil E. J., & Lynds, R. 1996, ApJ, 456, 174

Jiang, L., et al. 2002, in preparation

Kennicutt, R. C. 1984, ApJ, 287, 116

Kennicutt, R. C. 1988, ApJ, 334, 144

Kennicutt, R. C., & Chu Y. 1988, AJ, 95, 720

Kron, G. E., & Mayall, N. U. 1960, AJ, 65, 581

Landolt, A. U. 1983, AJ, 88, 439

Landolt, A. U. 1992, AJ, 104, 340

Ma, J., et al. 2001, AJ, 122, 1796

Ma, J., Zhou, X., Chen, J., Wu, H., Jiang, Z., Xue, S., & Zhu, J. 2002a, A&A, 385, 404

Ma, J., et al. 2002b, AJ, in press

Mayya, Y. D. 1994, AJ, 108, 1276

Melnick, J., & D’Odorico, S. 1978, A&AS, 34, 249

Miller, B. W., & Hodge, P. 1996, ApJ, 458, 467

Oey, M. S., & Kennicutt, R. C. 1997, MNRAS, 291, 827

Pellet, A., Astier, N., Viale. A., Courtès, G., Maucherat, A., Monnet, G., & Simien, F., 1978, A&AS, 31, 439

Petit, H., Sivan, J. P., & Karachentsev, I. D. 1988 A&AS, 74, 475

Viallefond, F., Donas, J., & Goss, W. M. 1983, A&A, 119, 185

Viallefond, F., & Goss, W. M. 1986, A&A, 154, 357

Walterbos, R. A. M., & Braun, R. 1992, A&AS, 92, 625

Walterbos, R. A. M. 2000, The Interstellar Medium in M31 and M33, Proceedings 232, 99

Wyder, T. K., Hodge, P. W., & Skelton B. P. 1997, PASP, 109, 927

Yan, H., et al. 2000, PASP, 112, 691

Zheng, Z. Y., et al. 1999, AJ, 117, 2757

Zhou, X., Jiang, Z., Xue, S., Wu, H., Ma, J., & Chen, J. 2001, CJAA, 1, 372

Zhou, X., et al. 2002, submitted

Table 3: SEDs of 145 HII Regions in M33

No.	03	04	05	06	07	08	09	10	11	12	13	14	15
(1)	(2)	(3)	(4)	(5)	(6)	(7)	(8)	(9)	(10)	(11)	(12)	(13)	(14)
1	16.87	16.88	16.61	16.91	16.88	17.00	16.29	17.04	17.09	17.04	17.12	16.95	17.38
	0.09	0.10	0.08	0.11	0.13	0.15	0.08	0.15	0.16	0.24	0.36	0.21	0.43
4	17.36	17.66	15.94	18.08	17.79	18.24	14.90	17.10	16.73	16.43	16.37	15.25	15.74
	0.23	0.31	0.07	0.51	0.48	0.73	0.04	0.26	0.19	0.22	0.30	0.07	0.16
5	15.98	15.94	15.55	16.01	16.06	16.18	15.56	16.31	16.42	16.38	16.51	16.26	16.45
	0.05	0.05	0.04	0.06	0.07	0.08	0.05	0.09	0.10	0.14	0.22	0.12	0.20
6	16.75	16.63	16.69	16.79	16.97	17.03	17.77	16.94	16.74	17.10	16.87	16.68	17.05
	0.12	0.11	0.13	0.14	0.20	0.22	0.43	0.20	0.17	0.36	0.42	0.23	0.46
7A	15.54	15.59	15.46	15.70	15.90	16.04	15.54	15.99	15.82	15.93	16.15	15.75	15.63
	0.04	0.05	0.04	0.05	0.08	0.09	0.06	0.08	0.07	0.12	0.21	0.10	0.12
7B	15.76	15.70	15.64	15.64	15.59	15.60	15.47	15.33	15.16	15.15	15.03	14.83	14.88
	0.05	0.05	0.05	0.05	0.05	0.05	0.05	0.04	0.04	0.05	0.07	0.04	0.06
8A	14.52	14.52	14.47	14.64	14.75	14.85	14.54	14.88	14.93	14.97	15.01	14.78	14.76
	0.02	0.02	0.03	0.03	0.04	0.04	0.03	0.04	0.05	0.07	0.10	0.06	0.08
9	16.26	16.21	16.03	16.17	16.17	16.24	16.06	16.17	16.02	16.14	16.21	15.84	15.99
	0.05	0.05	0.04	0.05	0.06	0.06	0.05	0.06	0.06	0.08	0.11	0.06	0.09
11	16.72	16.64	16.37	16.58	16.64	16.78	16.15	16.77	16.73	16.81	16.90	16.61	16.86
	0.10	0.10	0.09	0.10	0.14	0.16	0.09	0.15	0.15	0.25	0.38	0.19	0.34
12	17.63	17.56	17.43	17.60	17.58	17.64	17.16	17.63	17.76	17.76	17.90	17.83	17.57
	0.16	0.16	0.16	0.19	0.23	0.24	0.16	0.24	0.28	0.43	0.69	0.43	0.48
13	16.08	16.10	15.37	16.20	16.09	16.18	14.60	16.05	16.15	16.07	16.18	15.51	16.15
	0.07	0.07	0.04	0.09	0.10	0.11	0.03	0.09	0.10	0.15	0.24	0.09	0.22
17	15.80	15.81	15.43	15.84	15.83	15.92	14.81	15.90	15.87	15.77	15.76	15.40	15.77
	0.06	0.06	0.04	0.06	0.08	0.09	0.03	0.08	0.08	0.12	0.17	0.08	0.16
21	16.30	16.39	16.18	16.32	16.43	16.51	16.05	16.51	16.34	16.33	16.42	16.34	16.06
	0.10	0.11	0.10	0.11	0.15	0.17	0.11	0.16	0.14	0.22	0.36	0.21	0.24
25	14.46	14.15	13.93	13.91	13.72	13.70	13.51	13.59	13.60	13.53	13.50	13.43	13.47
	0.02	0.02	0.02	0.02	0.01	0.01	0.01	0.01	0.01	0.02	0.02	0.02	0.02

Table 3: Continued

No.	03	04	05	06	07	08	09	10	11	12	13	14	15	
	(1)	(2)	(3)	(4)	(5)	(6)	(7)	(8)	(9)	(10)	(11)	(12)	(13)	(14)
49	14.06	14.16	12.96	14.21	14.43	14.94	12.15	14.38	14.56	14.87	15.46	13.35	15.46	
	0.04	0.05	0.02	0.05	0.09	0.14	0.01	0.08	0.10	0.21	0.54	0.05	0.49	
55	17.89	17.65	17.05	17.26	16.86	16.92	16.32	16.67	16.67	16.48	16.64	16.31	16.46	
	0.21	0.17	0.11	0.13	0.12	0.13	0.07	0.10	0.10	0.14	0.23	0.11	0.19	
56	16.88	16.51	16.10	16.29	16.02	16.11	15.50	15.99	16.08	16.00	15.99	15.97	16.12	
	0.12	0.09	0.07	0.08	0.08	0.09	0.05	0.08	0.09	0.12	0.17	0.11	0.18	
58	17.80	17.76	17.56	17.54	17.77	17.96	17.50	18.08	18.04	18.10	18.43	18.38	18.49	
	0.16	0.15	0.14	0.14	0.22	0.26	0.16	0.28	0.27	0.47	0.93	0.57	0.91	
59	16.23	16.15	15.97	16.20	16.16	16.24	15.84	16.27	16.37	16.36	16.37	16.20	16.53	
	0.05	0.05	0.04	0.05	0.06	0.07	0.05	0.07	0.08	0.12	0.17	0.10	0.18	
60	17.15	17.24	16.65	17.43	17.44	17.73	16.21	17.72	17.92	17.51	17.91	17.34	17.73	
	0.15	0.17	0.11	0.23	0.29	0.38	0.09	0.37	0.46	0.48	0.99	0.39	0.79	
62	15.96	16.08	15.46	16.28	16.21	16.39	14.68	16.29	16.23	16.25	16.21	15.37	15.85	
	0.07	0.08	0.05	0.10	0.12	0.15	0.03	0.13	0.13	0.21	0.29	0.09	0.19	
63	16.87	17.01	16.08	16.94	16.87	17.18	15.50	17.21	17.03	16.82	17.06	16.13	16.73	
	0.16	0.19	0.09	0.20	0.24	0.32	0.07	0.32	0.28	0.36	0.64	0.18	0.44	
65	17.17	17.15	16.38	17.35	17.20	17.51	16.01	17.54	17.69	17.47	17.73	16.78	18.12	
	0.12	0.12	0.07	0.16	0.17	0.23	0.06	0.23	0.28	0.35	0.64	0.18	0.86	
77	15.15	15.19	14.88	15.30	15.26	15.35	14.24	15.28	15.30	15.29	15.22	15.02	15.31	
	0.04	0.04	0.03	0.05	0.05	0.06	0.02	0.06	0.06	0.09	0.12	0.07	0.12	
80	18.65	18.41	18.28	18.28	18.06	18.10	17.72	17.91	17.81	17.67	17.68	17.57	17.62	
	0.29	0.25	0.24	0.25	0.25	0.26	0.18	0.22	0.21	0.26	0.37	0.23	0.33	
83	15.66	15.65	15.50	15.77	15.74	15.89	15.35	15.84	15.72	15.72	15.62	15.27	15.34	
	0.04	0.04	0.04	0.05	0.06	0.06	0.04	0.06	0.06	0.08	0.11	0.05	0.08	
84	19.13	19.08	18.63	19.03	18.72	18.86	18.69	18.56	18.50	18.48	18.49	18.20	18.10	
	0.33	0.34	0.25	0.37	0.33	0.38	0.33	0.29	0.29	0.39	0.53	0.29	0.35	
85	16.22	16.18	16.03	16.13	16.02	16.09	15.57	15.92	15.78	15.67	15.64	15.40	15.32	
	0.07	0.07	0.06	0.07	0.08	0.09	0.05	0.07	0.07	0.09	0.12	0.07	0.09	

Table 3: Continued

No.	03	04	05	06	07	08	09	10	11	12	13	14	15	
	(1)	(2)	(3)	(4)	(5)	(6)	(7)	(8)	(9)	(10)	(11)	(12)	(13)	(14)
95A	16.48	16.47	15.90	16.51	16.36	16.47	15.26	16.38	16.47	16.39	16.55	15.81	16.53	
	0.09	0.09	0.06	0.11	0.12	0.13	0.04	0.12	0.13	0.20	0.34	0.11	0.31	
96	16.54	16.55	16.52	16.48	16.79	16.85	16.57	16.76	16.90	16.99	16.78	16.74	16.81	
	0.10	0.10	0.11	0.11	0.17	0.18	0.14	0.17	0.20	0.31	0.36	0.24	0.35	
97	16.98	16.96	16.94	17.20	17.11	17.31	16.78	17.45	17.70	17.70	17.46	17.38	18.09	
	0.11	0.11	0.12	0.15	0.17	0.21	0.13	0.23	0.30	0.45	0.52	0.32	0.86	
99	15.53	15.55	15.21	15.54	15.59	15.64	14.71	15.60	15.55	15.90	16.24	15.60	16.08	
	0.04	0.05	0.04	0.05	0.06	0.07	0.03	0.07	0.07	0.12	0.23	0.09	0.19	
100	14.49	14.46	14.25	14.49	14.47	14.55	13.66	14.53	14.55	14.51	14.56	14.25	14.43	
	0.04	0.04	0.03	0.04	0.05	0.05	0.02	0.05	0.05	0.08	0.12	0.06	0.10	
200	16.32	16.35	16.01	16.44	16.54	16.64	15.41	16.82	17.06	17.12	17.26	16.40	17.05	
	0.07	0.08	0.06	0.09	0.12	0.13	0.04	0.15	0.19	0.32	0.53	0.16	0.41	
201	16.91	17.10	16.67	17.16	17.09	17.40	16.44	17.34	17.43	17.17	17.46	16.86	16.94	
	0.15	0.18	0.13	0.21	0.24	0.33	0.13	0.30	0.33	0.42	0.79	0.29	0.46	
204	14.48	14.46	14.33	14.37	14.35	14.40	14.21	14.33	14.29	14.25	14.21	14.03	14.04	
	0.03	0.02	0.02	0.02	0.03	0.03	0.03	0.03	0.03	0.04	0.06	0.03	0.05	
205	14.29	14.21	14.09	14.05	14.04	14.07	14.00	14.00	13.96	13.93	13.89	13.75	13.77	
	0.02	0.02	0.02	0.02	0.02	0.02	0.02	0.02	0.02	0.03	0.05	0.03	0.04	
209	15.72	15.71	15.56	15.77	15.91	16.00	15.40	15.96	15.85	15.77	15.81	15.51	15.46	
	0.06	0.06	0.06	0.07	0.09	0.10	0.06	0.10	0.09	0.13	0.20	0.10	0.14	
211	17.72	17.77	17.49	17.81	17.80	17.88	16.80	17.90	18.08	18.11	18.08	17.59	18.39	
	0.13	0.14	0.12	0.15	0.20	0.21	0.08	0.21	0.25	0.43	0.62	0.25	0.76	
214	16.28	16.34	15.73	16.33	16.20	16.29	14.80	16.08	16.08	16.01	15.90	15.27	15.74	
	0.05	0.06	0.04	0.06	0.07	0.07	0.02	0.06	0.06	0.09	0.12	0.04	0.10	
216	16.49	16.45	15.89	16.27	16.29	16.40	15.54	16.19	16.08	16.01	15.94	15.63	15.66	
	0.11	0.11	0.07	0.10	0.13	0.15	0.07	0.12	0.11	0.18	0.25	0.12	0.18	
217	15.57	15.56	14.80	15.53	15.51	15.60	14.64	15.54	15.53	15.51	15.56	15.15	15.49	
	0.06	0.06	0.03	0.06	0.08	0.08	0.03	0.07	0.07	0.13	0.20	0.08	0.17	

Table 3: Continued

No.	03	04	05	06	07	08	09	10	11	12	13	14	15	
	(1)	(2)	(3)	(4)	(5)	(6)	(7)	(8)	(9)	(10)	(11)	(12)	(13)	(14)
224	17.69	17.62	17.43	17.64	17.52	17.69	16.78	17.30	17.10	16.97	16.84	16.40	16.45	
	0.21	0.20	0.18	0.22	0.26	0.31	0.13	0.21	0.18	0.27	0.36	0.15	0.23	
226	17.41	17.37	17.12	17.33	17.18	17.12	16.34	16.65	16.43	16.31	16.22	16.08	15.99	
	0.15	0.15	0.13	0.15	0.18	0.17	0.08	0.11	0.09	0.14	0.19	0.10	0.14	
230	15.61	15.56	15.26	15.41	15.28	15.35	14.91	15.25	15.23	15.10	15.18	14.94	15.03	
	0.06	0.06	0.05	0.06	0.07	0.07	0.05	0.06	0.06	0.10	0.16	0.08	0.12	
231	17.98	17.96	17.63	18.09	17.97	18.10	17.02	17.92	18.02	17.90	17.88	17.56	17.99	
	0.19	0.19	0.15	0.22	0.27	0.31	0.11	0.25	0.27	0.44	0.65	0.30	0.65	
232	17.18	17.16	16.98	17.15	16.98	17.01	16.59	16.76	16.75	16.66	16.58	16.45	16.43	
	0.11	0.10	0.09	0.11	0.12	0.13	0.08	0.09	0.10	0.15	0.21	0.12	0.17	
233	17.32	17.24	16.71	17.14	16.81	16.87	15.72	16.28	15.86	15.74	15.78	15.47	15.42	
	0.24	0.22	0.15	0.21	0.22	0.23	0.08	0.13	0.09	0.14	0.22	0.10	0.15	
234	16.09	16.13	16.07	16.24	16.29	16.39	16.15	16.50	16.59	16.57	16.70	16.59	16.67	
	0.05	0.05	0.05	0.06	0.08	0.09	0.07	0.09	0.10	0.17	0.28	0.16	0.25	
236	16.66	16.69	16.67	16.90	16.90	17.02	16.63	17.12	17.25	17.17	17.41	17.13	17.90	
	0.09	0.09	0.10	0.12	0.16	0.18	0.12	0.18	0.21	0.35	0.66	0.31	0.95	
237	16.01	16.06	15.62	16.11	16.06	16.15	15.49	16.05	16.03	15.97	16.00	15.69	15.81	
	0.06	0.07	0.05	0.07	0.09	0.10	0.05	0.09	0.09	0.15	0.23	0.11	0.18	
238	16.20	16.21	15.94	16.28	16.27	16.43	15.80	16.51	16.63	16.64	16.73	16.61	16.83	
	0.05	0.05	0.04	0.05	0.07	0.08	0.04	0.08	0.09	0.15	0.25	0.14	0.25	
240	17.83	17.86	16.95	17.98	17.85	18.04	16.71	17.93	18.02	17.95	18.02	17.34	17.92	
	0.15	0.15	0.08	0.18	0.22	0.26	0.08	0.22	0.24	0.40	0.65	0.21	0.54	
241	18.07	18.38	17.62	18.28	18.20	18.15	17.18	18.32	18.48	18.17	18.46	18.10	18.20	
	0.17	0.21	0.12	0.21	0.26	0.25	0.10	0.27	0.32	0.44	0.87	0.38	0.62	
242	16.66	16.64	16.58	16.64	16.72	16.82	16.77	16.80	16.76	16.73	16.79	16.54	16.49	
	0.09	0.09	0.09	0.09	0.13	0.15	0.13	0.14	0.13	0.23	0.36	0.18	0.25	
243	16.50	16.54	16.22	16.60	16.66	16.78	16.36	16.91	17.11	17.17	17.26	16.98	17.35	
	0.08	0.08	0.06	0.09	0.12	0.14	0.09	0.15	0.18	0.34	0.57	0.26	0.56	

Table 3: Continued

No.	03	04	05	06	07	08	09	10	11	12	13	14	15	
	(1)	(2)	(3)	(4)	(5)	(6)	(7)	(8)	(9)	(10)	(11)	(12)	(13)	(14)
258	17.52	17.21	16.28	16.97	16.57	16.48	15.74	16.17	16.09	15.97	15.94	15.66	15.86	
	0.20	0.15	0.07	0.13	0.13	0.12	0.06	0.08	0.08	0.13	0.19	0.09	0.16	
263	16.13	16.08	15.87	16.00	15.87	15.87	15.15	15.54	15.33	15.24	15.23	14.90	14.93	
	0.11	0.10	0.09	0.10	0.12	0.13	0.06	0.09	0.07	0.13	0.19	0.08	0.13	
264	16.13	16.14	15.81	16.16	16.23	16.30	15.70	16.41	16.52	16.46	16.54	16.41	16.54	
	0.06	0.06	0.05	0.07	0.10	0.11	0.06	0.11	0.12	0.21	0.35	0.18	0.32	
268	15.03	14.98	14.85	14.95	14.96	15.01	14.96	15.06	15.12	15.11	15.11	15.07	15.09	
	0.02	0.02	0.02	0.02	0.03	0.03	0.03	0.03	0.03	0.05	0.08	0.05	0.07	
272	16.09	16.02	15.43	15.94	15.83	15.83	15.04	15.74	15.75	15.64	15.67	15.35	15.65	
	0.07	0.07	0.05	0.07	0.09	0.09	0.04	0.07	0.07	0.13	0.20	0.09	0.18	
274	14.43	14.37	13.80	14.31	14.32	14.37	13.65	14.27	14.29	14.21	14.26	14.03	14.32	
	0.04	0.04	0.02	0.04	0.05	0.05	0.03	0.04	0.05	0.08	0.13	0.06	0.13	
275	17.77	17.72	17.44	17.76	17.81	17.81	17.22	17.78	17.71	17.85	17.70	17.72	17.29	
	0.16	0.16	0.13	0.17	0.25	0.25	0.13	0.22	0.21	0.46	0.61	0.37	0.38	
276	16.56	16.29	16.03	16.11	15.87	15.98	15.91	15.99	16.02	15.86	15.90	15.79	16.18	
	0.16	0.12	0.10	0.11	0.12	0.14	0.12	0.13	0.13	0.21	0.34	0.18	0.40	
277	13.59	13.46	13.09	13.30	13.27	13.28	12.85	13.21	13.24	13.19	13.20	13.07	13.17	
	0.01	0.01	0.01	0.01	0.02	0.02	0.01	0.01	0.01	0.02	0.03	0.02	0.03	
278	18.49	18.36	17.97	18.13	17.80	17.83	17.42	17.85	17.91	17.75	17.83	17.62	17.90	
	0.26	0.23	0.18	0.20	0.20	0.21	0.14	0.20	0.22	0.32	0.51	0.26	0.50	
280	14.86	14.91	13.24	15.00	14.97	15.17	13.54	15.10	15.26	15.22	15.44	14.50	15.47	
	0.03	0.03	0.01	0.03	0.04	0.05	0.01	0.05	0.05	0.09	0.18	0.05	0.16	
285	19.25	19.06	18.74	18.84	18.54	18.68	18.49	18.47	18.40	18.22	18.14	18.23	18.42	
	0.53	0.44	0.36	0.38	0.41	0.47	0.36	0.36	0.35	0.54	0.76	0.50	0.90	
288	15.56	15.59	15.11	15.66	15.70	15.79	15.04	15.74	15.68	15.63	15.60	15.35	15.48	
	0.06	0.06	0.04	0.06	0.09	0.10	0.05	0.09	0.09	0.15	0.22	0.11	0.18	
290A	16.10	16.08	15.06	16.26	16.16	16.45	15.26	16.51	16.65	16.64	16.75	16.27	17.06	
	0.08	0.08	0.04	0.09	0.12	0.16	0.05	0.15	0.18	0.32	0.53	0.21	0.65	

Table 3: Continued

No.	03	04	05	06	07	08	09	10	11	12	13	14	15	
	(1)	(2)	(3)	(4)	(5)	(6)	(7)	(8)	(9)	(10)	(11)	(12)	(13)	(14)
608	16.51	16.27	15.99	15.94	15.56	15.48	14.87	14.89	14.50	14.32	14.22	14.03	13.95	
	0.15	0.12	0.10	0.09	0.09	0.09	0.05	0.05	0.04	0.05	0.07	0.04	0.05	
609	15.38	15.40	15.24	15.37	15.43	15.46	15.05	15.45	15.43	15.44	15.38	15.30	15.33	
	0.05	0.06	0.05	0.06	0.08	0.09	0.05	0.08	0.08	0.14	0.20	0.12	0.18	
618	17.75	17.59	17.03	17.40	17.12	17.14	16.35	17.04	17.12	16.98	17.00	16.77	16.83	
	0.19	0.16	0.11	0.14	0.15	0.16	0.07	0.13	0.15	0.24	0.37	0.18	0.29	
623	15.37	15.44	14.03	15.50	15.50	15.65	14.15	15.51	15.67	15.60	15.57	14.87	15.77	
	0.04	0.05	0.02	0.05	0.07	0.08	0.02	0.06	0.07	0.13	0.19	0.06	0.21	
624	16.47	16.41	15.97	16.27	16.14	16.11	15.52	15.85	15.54	15.47	15.43	15.01	15.09	
	0.06	0.06	0.04	0.05	0.06	0.06	0.03	0.05	0.04	0.06	0.08	0.04	0.06	
625	16.71	16.68	16.35	16.61	16.57	16.53	15.97	16.29	15.98	15.90	15.84	15.45	15.52	
	0.07	0.07	0.06	0.07	0.09	0.09	0.05	0.07	0.05	0.09	0.12	0.05	0.08	
626	15.34	15.31	14.93	15.26	15.24	15.33	14.69	15.30	15.31	15.33	15.44	15.20	15.37	
	0.05	0.05	0.04	0.05	0.07	0.08	0.04	0.07	0.07	0.13	0.22	0.11	0.19	
629	16.34	16.35	15.90	16.44	16.40	16.52	15.75	16.52	16.55	16.43	16.55	16.11	16.43	
	0.05	0.05	0.04	0.06	0.08	0.09	0.04	0.08	0.08	0.13	0.21	0.09	0.18	
631	17.26	17.26	16.44	17.37	17.29	17.43	16.15	17.35	17.42	17.35	17.47	17.03	17.48	
	0.14	0.14	0.08	0.17	0.21	0.24	0.07	0.21	0.23	0.38	0.62	0.26	0.58	
632	14.99	14.96	14.81	14.94	14.98	15.05	14.64	15.11	15.17	15.18	15.27	15.15	15.38	
	0.04	0.04	0.03	0.04	0.05	0.06	0.04	0.06	0.06	0.10	0.17	0.09	0.17	
635	15.09	14.89	14.75	14.68	14.67	14.65	14.57	14.63	14.60	14.58	14.57	14.60	14.57	
	0.04	0.03	0.03	0.03	0.03	0.03	0.03	0.03	0.03	0.05	0.08	0.05	0.07	
637	16.35	16.07	14.87	15.96	15.67	15.65	14.89	15.55	15.50	15.41	15.42	15.19	15.54	
	0.14	0.10	0.04	0.10	0.11	0.11	0.05	0.09	0.09	0.15	0.23	0.11	0.24	
638	15.35	15.39	13.24	15.23	15.26	15.41	13.67	15.34	15.44	15.30	15.43	14.42	15.45	
	0.05	0.06	0.01	0.05	0.07	0.09	0.02	0.07	0.08	0.13	0.23	0.05	0.21	
641	15.63	15.66	14.87	15.83	15.77	15.93	14.79	16.04	16.07	16.04	16.27	15.63	16.30	
	0.09	0.10	0.05	0.12	0.16	0.19	0.06	0.19	0.20	0.37	0.70	0.23	0.67	

Table 3: Continued

No.	03	04	05	06	07	08	09	10	11	12	13	14	15	
	(1)	(2)	(3)	(4)	(5)	(6)	(7)	(8)	(9)	(10)	(11)	(12)	(13)	(14)
664	15.72	15.75	15.39	15.83	15.92	16.08	15.37	16.19	16.14	16.22	15.85	15.93	16.13	
	0.08	0.08	0.06	0.09	0.14	0.16	0.08	0.17	0.16	0.32	0.34	0.22	0.41	
665	15.58	15.53	15.50	15.49	15.46	15.55	15.44	15.56	15.46	15.37	15.40	15.15	15.13	
	0.09	0.08	0.09	0.08	0.11	0.12	0.10	0.12	0.11	0.17	0.26	0.13	0.19	
667	15.59	15.59	15.44	15.67	15.72	15.82	15.14	15.83	15.90	15.85	15.96	15.61	15.82	
	0.06	0.06	0.05	0.07	0.09	0.10	0.05	0.10	0.10	0.17	0.28	0.13	0.23	
680	12.32	12.63	11.26	12.39	12.39	12.62	10.76	12.52	12.61	12.53	12.69	11.82	12.71	
	0.01	0.01	0.00	0.01	0.01	0.02	0.00	0.02	0.02	0.03	0.05	0.01	0.04	
684	16.99	17.06	16.90	17.79	16.74	16.87	15.56	16.83	16.77	16.44	16.68	16.37	16.48	
	0.21	0.23	0.21	0.48	0.25	0.29	0.08	0.26	0.25	0.33	0.61	0.28	0.47	
685	17.06	17.22	16.83	17.63	17.32	17.59	15.87	17.55	17.57	17.31	17.51	16.86	17.37	
	0.14	0.16	0.13	0.26	0.26	0.34	0.07	0.31	0.32	0.45	0.80	0.27	0.65	
687	16.42	16.07	15.74	15.83	15.49	15.45	14.93	15.24	15.16	15.07	15.01	14.87	14.90	
	0.11	0.08	0.07	0.07	0.07	0.07	0.04	0.05	0.05	0.08	0.11	0.06	0.09	
688	14.72	14.69	14.60	14.66	14.69	14.77	14.67	14.83	14.89	14.86	14.85	14.79	14.91	
	0.02	0.02	0.02	0.03	0.03	0.03	0.03	0.03	0.04	0.06	0.08	0.05	0.08	
689	15.50	15.51	15.46	15.55	15.59	15.70	15.55	15.61	15.52	15.54	15.53	15.46	15.38	
	0.04	0.04	0.05	0.05	0.06	0.07	0.06	0.06	0.06	0.09	0.13	0.08	0.11	
692	17.53	17.32	16.96	17.14	16.84	16.90	16.35	16.73	16.62	16.42	16.37	16.25	16.41	
	0.24	0.20	0.16	0.18	0.18	0.20	0.11	0.16	0.15	0.21	0.29	0.17	0.28	
696	16.92	16.90	16.76	16.96	16.98	17.05	16.25	17.09	17.08	17.11	17.11	16.79	16.91	
	0.11	0.11	0.10	0.12	0.16	0.18	0.08	0.17	0.18	0.30	0.45	0.21	0.34	
704	15.17	15.18	15.08	15.13	15.20	15.32	15.31	15.47	15.61	15.73	15.89	15.87	15.77	
	0.06	0.06	0.06	0.07	0.09	0.11	0.10	0.12	0.14	0.25	0.43	0.26	0.35	
707	16.29	16.16	15.89	16.09	16.14	16.29	15.66	16.20	16.17	16.29	16.33	16.22	15.83	
	0.14	0.12	0.11	0.13	0.17	0.20	0.11	0.18	0.18	0.31	0.46	0.27	0.27	
709	15.40	15.33	15.22	15.28	15.34	15.42	15.05	15.51	15.56	15.43	15.69	15.64	16.48	
	0.06	0.05	0.05	0.05	0.07	0.08	0.06	0.08	0.09	0.13	0.25	0.15	0.47	

Table 3: Continued

No.	03	04	05	06	07	08	09	10	11	12	13	14	15	
	(1)	(2)	(3)	(4)	(5)	(6)	(7)	(8)	(9)	(10)	(11)	(12)	(13)	(14)
720	16.74	16.65	16.32	16.74	16.62	16.76	16.01	16.73	16.84	16.74	16.75	16.72	16.67	
	0.09	0.09	0.07	0.10	0.12	0.14	0.07	0.13	0.14	0.21	0.32	0.20	0.27	
728	17.46	17.54	17.38	17.69	17.47	17.74	17.19	17.65	17.25	17.23	17.35	16.95	16.97	
	0.21	0.22	0.21	0.27	0.31	0.40	0.22	0.34	0.24	0.44	0.75	0.31	0.49	
734	15.90	15.94	15.81	15.95	16.00	16.04	15.60	15.94	15.78	15.75	15.69	15.36	15.47	
	0.05	0.05	0.05	0.06	0.08	0.08	0.05	0.07	0.06	0.10	0.14	0.07	0.11	
740	15.89	15.97	15.20	15.95	15.84	16.03	14.60	15.94	15.97	15.93	16.11	15.35	16.17	
	0.06	0.07	0.04	0.07	0.09	0.10	0.03	0.09	0.09	0.16	0.29	0.09	0.28	
741	18.91	18.87	18.59	18.55	18.00	18.02	17.55	17.43	17.18	17.05	16.87	16.56	16.63	
	0.29	0.28	0.24	0.22	0.19	0.19	0.12	0.11	0.09	0.13	0.17	0.08	0.12	
745	18.36	18.24	17.37	18.44	18.30	18.50	16.85	18.31	18.18	18.12	17.98	17.67	17.95	
	0.25	0.22	0.12	0.28	0.35	0.43	0.09	0.33	0.30	0.53	0.70	0.32	0.63	
746	17.53	17.45	17.22	17.36	17.47	17.51	17.13	17.34	17.13	17.07	17.27	16.87	16.71	
	0.23	0.22	0.19	0.22	0.32	0.33	0.22	0.27	0.23	0.37	0.65	0.28	0.36	
748	17.43	16.68	16.33	16.20	15.63	15.43	15.06	15.03	14.85	14.65	14.61	14.45	14.43	
	0.13	0.07	0.06	0.05	0.04	0.04	0.03	0.03	0.02	0.03	0.04	0.02	0.03	
749	15.49	15.50	15.24	15.61	15.61	15.69	14.72	15.73	16.09	15.73	15.72	15.44	15.74	
	0.04	0.04	0.04	0.05	0.06	0.07	0.03	0.07	0.09	0.12	0.18	0.08	0.17	
752	17.17	17.19	16.81	17.20	17.21	17.36	16.33	17.18	17.06	17.02	17.19	17.23	17.05	
	0.14	0.14	0.11	0.14	0.20	0.24	0.09	0.19	0.17	0.31	0.54	0.34	0.43	
753	17.88	17.81	17.63	17.76	17.93	18.03	17.84	18.07	18.05	18.21	18.21	18.19	18.18	
	0.15	0.14	0.13	0.14	0.23	0.25	0.19	0.24	0.24	0.51	0.77	0.45	0.68	
755	15.81	15.80	15.34	15.94	15.86	16.12	15.33	16.31	16.38	16.38	16.50	16.30	16.77	
	0.07	0.07	0.05	0.08	0.10	0.13	0.06	0.14	0.15	0.29	0.50	0.25	0.58	
756	16.87	16.81	16.33	16.73	16.53	16.59	15.75	16.45	16.23	16.07	16.08	15.76	15.97	
	0.13	0.12	0.09	0.11	0.14	0.15	0.06	0.12	0.10	0.16	0.24	0.11	0.20	
758	16.27	16.26	15.95	16.31	16.39	16.52	15.90	16.59	16.60	16.60	16.72	16.01	16.18	
	0.09	0.09	0.07	0.10	0.15	0.17	0.09	0.17	0.17	0.30	0.51	0.16	0.29	

Table 3: Continued

No.	03	04	05	06	07	08	09	10	11	12	13	14	15
(1)	(2)	(3)	(4)	(5)	(6)	(7)	(8)	(9)	(10)	(11)	(12)	(13)	(14)
1502	15.26	15.22	15.11	15.11	15.13	15.21	15.10	15.21	15.17	15.14	15.25	15.22	15.25
	0.05	0.05	0.05	0.05	0.06	0.07	0.06	0.07	0.06	0.10	0.16	0.10	0.15

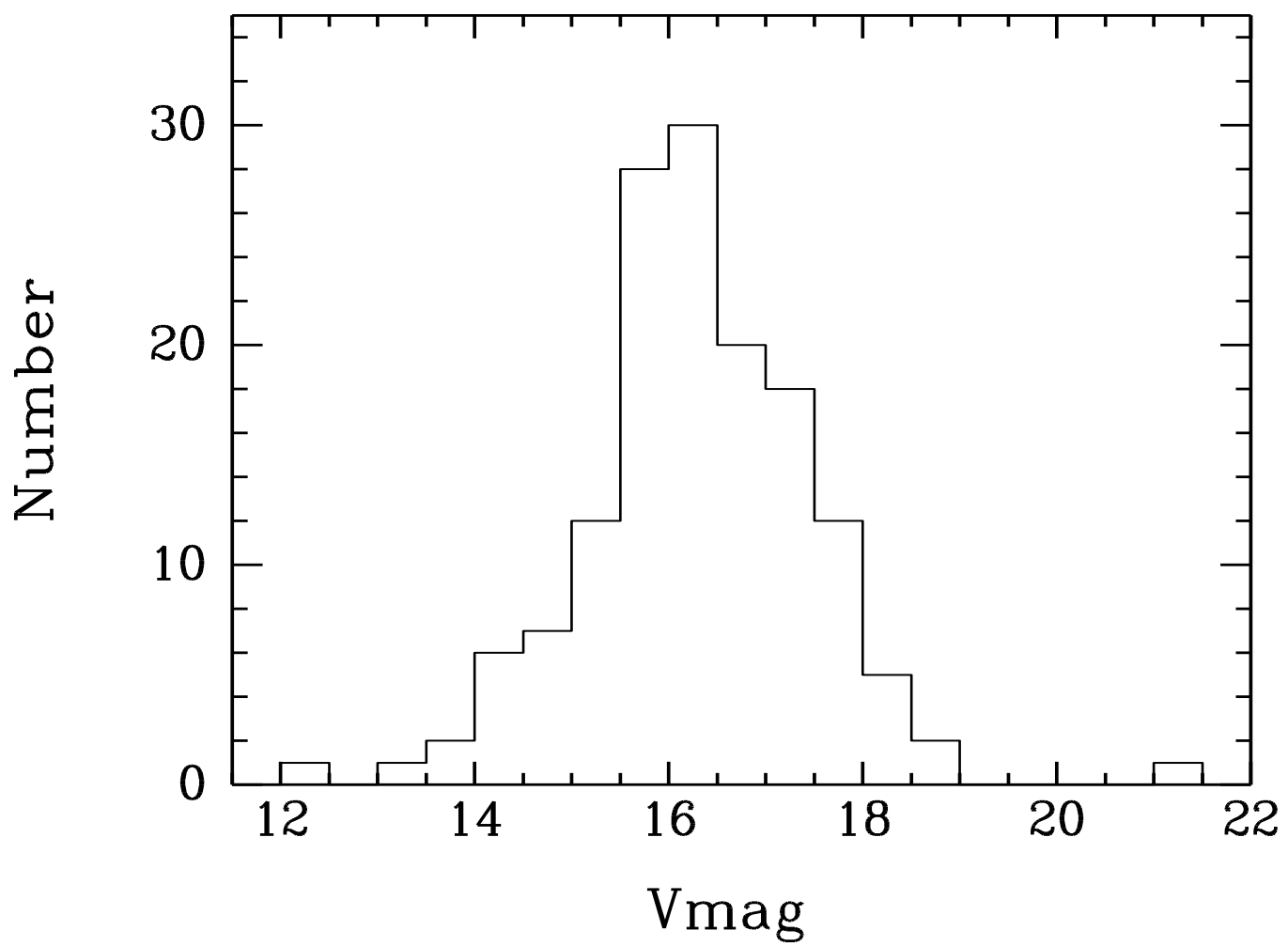


Fig. 1.— Histogram of magnitudes in computed V band for 145 HII regions.

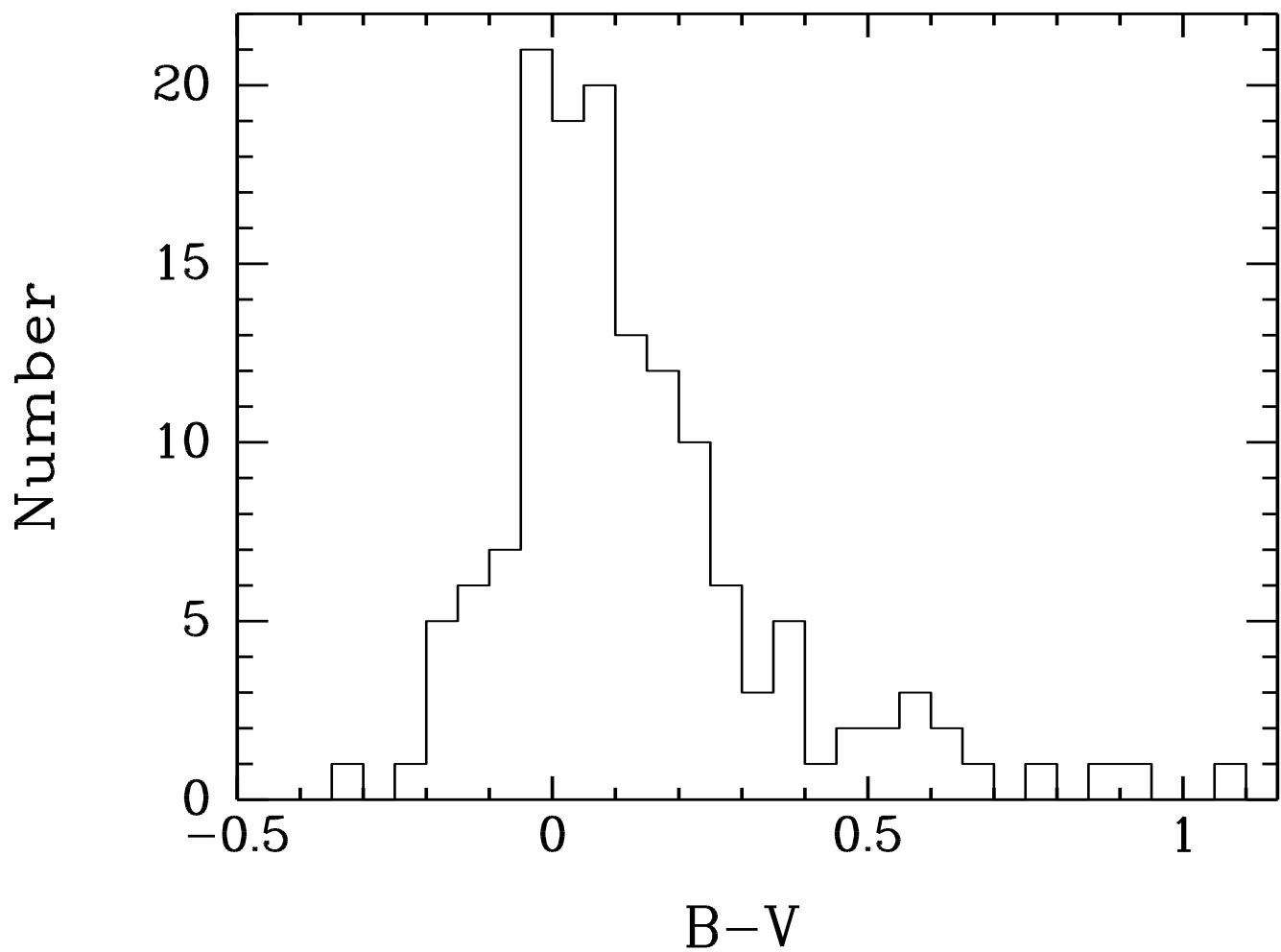


Fig. 2.— Histogram of computed  $B-V$  color for 145 HII regions.

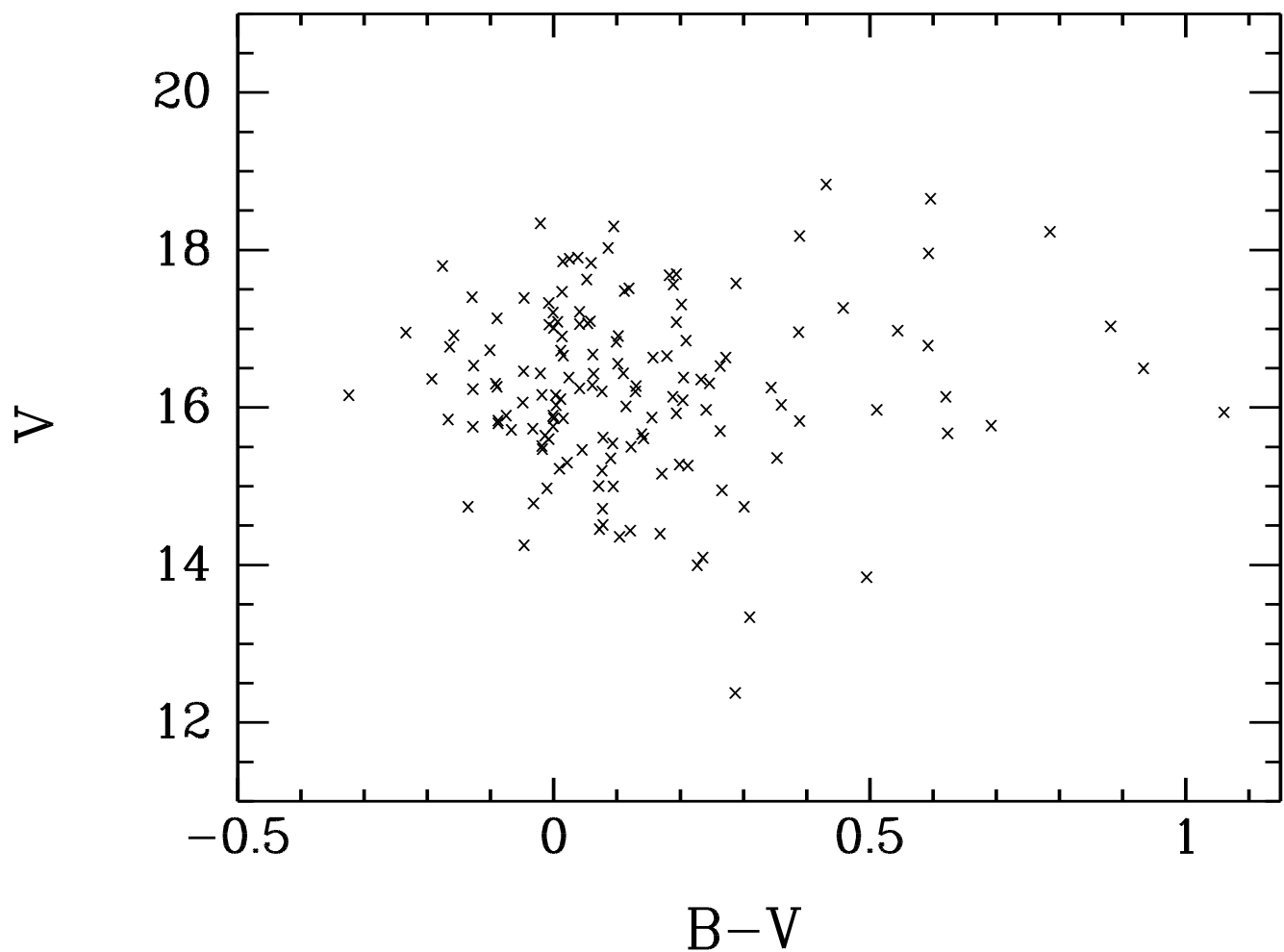


Fig. 3.— The color-magnitude diagram for 145 HII regions.

This figure "jiangfig4a.jpg" is available in "jpg" format from:

<http://arxiv.org/ps/astro-ph/0209204v1>

This figure "jiangfig4b.jpg" is available in "jpg" format from:

<http://arxiv.org/ps/astro-ph/0209204v1>

This figure "jiangfig4c.jpg" is available in "jpg" format from:

<http://arxiv.org/ps/astro-ph/0209204v1>

This figure "jiangfig4d.jpg" is available in "jpg" format from:

<http://arxiv.org/ps/astro-ph/0209204v1>

This figure "jiangfig4e.jpg" is available in "jpg" format from:

<http://arxiv.org/ps/astro-ph/0209204v1>

This figure "jiangfig5.jpg" is available in "jpg" format from:

<http://arxiv.org/ps/astro-ph/0209204v1>

This figure "jiangfig6a.jpg" is available in "jpg" format from:

<http://arxiv.org/ps/astro-ph/0209204v1>

This figure "jiangfig6b.jpg" is available in "jpg" format from:

<http://arxiv.org/ps/astro-ph/0209204v1>

This figure "jiangfig6c.jpg" is available in "jpg" format from:

<http://arxiv.org/ps/astro-ph/0209204v1>

This figure "jiangfig6d.jpg" is available in "jpg" format from:

<http://arxiv.org/ps/astro-ph/0209204v1>

This figure "jiangfig6e.jpg" is available in "jpg" format from:

<http://arxiv.org/ps/astro-ph/0209204v1>

This figure "jiangfig6f.jpg" is available in "jpg" format from:

<http://arxiv.org/ps/astro-ph/0209204v1>

This figure "jiangfig6g.jpg" is available in "jpg" format from:

<http://arxiv.org/ps/astro-ph/0209204v1>

This figure "jiangfig6h.jpg" is available in "jpg" format from:

<http://arxiv.org/ps/astro-ph/0209204v1>

This figure "jiangfig6i.jpg" is available in "jpg" format from:

<http://arxiv.org/ps/astro-ph/0209204v1>

This figure "jiangfig6j.jpg" is available in "jpg" format from:

<http://arxiv.org/ps/astro-ph/0209204v1>